# Mrs2p Forms a High Conductance $Mg^{2+}$ Selective Channel in Mitochondria

Rainer Schindl,* Julian Weghuber,† Christoph Romanin,* and Rudolf J. Schweyen†
*Institute for Biophysics, University of Linz, Linz, Austria; and †Max F. Perutz Laboratories, Department of Genetics, University of Vienna, Vienna, Austria

ABSTRACT Members of the CorA-Mrs2-Alr1 superfamily of $Mg^{2+}$ transporters are ubiquitous among pro- and eukaryotes. The crystal structure of a bacterial CorA protein has recently been solved, but the mode of ion transport of this protein family remained obscure. Using single channel patch clamping we unequivocally show here that the mitochondrial Mrs2 protein forms a $Mg^{2+}$-selective channel of high conductance (155 pS). It has an open probability of ~60% in the absence of $Mg^{2+}$ at the matrix site, which decreases to ~20% in its presence. With a lower conductance (~45 pS) the Mrs2 channel is also permeable for $Ni^{2+}$, whereas no permeability has been observed for either $Ca^{2+}$, $Mn^{2+}$, or $Co^{2+}$. Mutational changes in key domains of Mrs2p are shown either to abolish its $Mg^{2+}$ transport or to change its characteristics toward more open and partly deregulated states. We conclude that Mrs2p forms a high conductance $Mg^{2+}$ selective channel that controls $Mg^{2+}$ influx into mitochondria by an intrinsic negative feedback mechanism.

## INTRODUCTION

Common features of bacterial CorA proteins and eukaryotic Mrs2 and Alr1 proteins are the presence of two adjacent transmembrane domains (TM), of which the first one ends with a gly-met-asn (GMN) motif, and additional secondary structures (1–4). Several of these proteins have been shown to form homooligomers in their cognate membranes and to transport $Mg^{2+}$ (1,5–7). Based on these conserved features they are regarded as forming a superfamily of $Mg^{2+}$ transport proteins.

CorA has been the first characterized member of this superfamily. In *Salmonella typhimurium* cells CorA (St-CorA) constitutes the major transport protein for $Mg^{2+}$ uptake driven by the inside negative membrane potential (5,6). Recently published crystal structures of CorA of the eubacterium *Thermotoga maritima* (Tm-CorA) reveal a homopentameric cone-shaped complex (4). The tip of the cone is formed by the two TM helices, one of which forms the pore and extends toward the major, N-terminal part of CorA, folded into a large funnel-shaped structure. Binding of $Mg^{2+}$ to sites in this funnel structure is proposed to elicit conformational reorientations that are transmitted to the pore to control its $Mg^{2+}$ transport status. Prominent features of the outer side of the membrane pore, forming the $Mg^{2+}$ entry side, are the GMN motif at the end of the pore-forming TM domain and a short loop with a surplus of negative charges (4,8,9). Although sequence and structural comparisons clearly reveal Tm-CorA to be related to functionally characterized $Mg^{2+}$ transporters, a direct demonstration of its transport activity is still lacking.

Most eukaryotic genomes encode distant homologs of bacterial CorA proteins, which can be grouped into the Alr1 and Mrs2 subfamilies of CorA-related proteins (2). They mostly lack sequence similarity except the GMN motif, but predicted secondary structures of their core sequences align well with those of CorA proteins, strongly suggesting that they indeed share with CorA essential parts of their higher order structures (4). Unrelated to the CorA/Mrs2/Alr1 superfamily of $Mg^{2+}$ transporters are the TRPM6/TRPM7 $Mg^{2+}$ channel proteins localized in the mammalian plasma membrane (10), the MgtE/SLC41a family with representatives in bacteria and mammalian (11), as well as some further candidate $Mg^{2+}$ transport proteins (12).

The best characterized of the eukaryotic CorA-related proteins is the yeast Mrs2 protein (yMrs2p). A long N-terminal as well as a short C-terminal sequence are shown to be oriented toward the inner side of the membrane leaving the short loop connecting the TM domains protruding to its outside (13,14). Its membrane orientation thus is like that of Tm-CorA (4,8,9). Yeast knock-out mutants (*mrs2*Δ) are mitochondrially defective, but viable in fermentable substrates. Various other Mrs2 proteins have been shown to partially complement growth defects of *mrs2*Δ cells, including a second CorA-related yeast protein, named Lpe10p, as well as a single human Mrs2p (13,15,16), some plant Mrs2 proteins and CorA of *S. typhimurium*.

Here we present electrophysiological data that characterize in detail Mrs2p-mediated ion currents. Large single channel $Mg^{2+}$ currents were found to correlate with the

*Submitted May 8, 2007, and accepted for publication June 29, 2007.*

Rainer Schindl and Julian Weghuber contributed equally to this work.

Address reprint requests to Christoph Romanin, University of Linz, Linz, Austria. Tel.: 4373224689272; E-mail: christoph.romanin@jku.at; or to Rudolf J. Schweyen, MFPL, University of Vienna, Vienna, Austria. Tel.: 431427754604; E-mail: rudolf.schweyen@univie.ac.at.

Julian Weghuber's present address is Institute for Biophysics, University of Linz, Linz, Austria.



Editor: Eduardo Perozo.


0006-3495/07/12/3872/12 $2.00

doi: 10.1529/biophysj.107.112318

expression levels of Mrs2p. Mutations in key domains of Mrs2p affected either gating or permeation. Mrs2p channels were selective for $Mg^{2+}$ over $Ni^{2+}$ with no permeability for $Ca^{2+}$, $Mn^{2+}$, and $Co^{2+}$. Matrix $Mg^{2+}$ regulated Mrs2p activity implying an intrinsic negative feedback mechanism. Combined with previous findings (7,13,15–17) these data indicate that Mrs2p oligomers constitute the high conductance $Mg^{2+}$-selective channel of mitochondria.

## MATERIALS AND METHODS

### Yeast strains, growth media, and genetic procedures

The yeast *Saccharomyces cerevisiae* DBY747 wild-type strain, the isogenic *mrs2*Δ deletion strain (DBY *mrs2-1*), and the *mrs2*Δ, *lpe10*Δ double disruptant (DBY747 *mrs2-2, lpe10-2*) have been described previously (13,17,18). Yeast cells were grown in rich medium ((yeast peptone dextrose (YPD)) 1% yeast extract, 2% peptone, Becton Dickinson, Franklin Lakes, NJ) with 2% glucose (AppliChem, Cheshire, CT) as a carbon source to early stationary phase. The plasmid construct YEp351 Mrs2-HA (13) was digested with *Sac*I and *Sph*I and cloned into an empty YEp112 vector digested with the same restriction enzymes. The resulting YEp112 Mrs2-HA construct was digested with *Not*I, dephosphorylated (Antarctic Phosphatase, New England Biolabs, Beverly, MA), and a cassette coding for the myc epitope tag was cloned in frame with the *Mrs2* gene at the *Not*I site, resulting in the construct YEp112 MRS2-myc. The construct pVT-103U MRS2 has been previously described (7). To generate two Mrs2p variants mutated in predicted coiled-coil regions of the protein—Mrs2-HA(Δ277–282) and Mrs2-HA(ins207/208) (insertion of seven amino acids LNDLENE between E207 and V208; cf. Supplementary Fig. S1 and Supplementary Material for polymerase chain reaction primers)—overlap extension polymerase chain reaction according to Pogulis et al. (19) was used.

### Isolation of mitochondria and measurement of $[Mg^{2+}]_m$ by spectrofluorometry

The isolation of mitochondria by differential centrifugation and the ratiometric determination of intramitochondrial $Mg^{2+}$ concentrations ($[Mg^{2+}]_m$) dependent on various external concentrations ($[Mg^{2+}]_e$) has been performed as previously reported (7).

### Blue native gel electrophoresis

Mitochondria were isolated from an *mrs2*Δ strain expressing the MRS2-myc, MRS2-HA, MRS2-HA(Δ277–282), or MRS2-HA(ins207/208) constructs from a YEp multicopy vector. Mitochondria (80 μg) were extracted by addition of 40 μl extraction buffer (750 mM aminocaproic acid, 50 mM Bistris/HCl, pH 7.0), and laurylmaltoside to a final concentration of 1%. After incubation on ice for 30 min the samples were centrifuged at 45,000 × *g* for 30 min and the supernatant was supplemented with 1/4 vol of sample buffer (500 mM aminocaproic acid, 5% Serva blue G). The solubilized protein solution (25 μl) was analyzed by blue native (BN) electrophoresis on a 5–18% linear polyacrylamide gradient according to Schagger et al. (20). The gel was blotted onto a nitrocellulose membrane, which was then either stained with Coomassie blue reagent or analyzed by immunoblotting with a myc or an HA antiserum.

### Preparation of giant lipid vesicles

Asolectin lipids (Sigma-Aldrich, St. Louis, MO) were suspended in 10 ml of distilled water, at 100 mg/ml, by sonication for 3 min in a Sonoplus GM70 apparatus set at 70%. The almost transparent lipid suspension was diluted 10-fold with 10 mM HEPES, pH 7.4, 100 mM NaCl, and solid CHAPS was added to a final concentration of 1%. Lipid vesicles were formed by elimination of the detergent by exhaustive dialysis. The dialyzed sample was stored at −80°C.

The formation of giant liposomes has been performed according to (21,22). Submitochondrial particles (SMPs) were prepared as previously reported (6). The SMP membrane aliquot (1 ml) (1 mg protein per ml) was mixed with 800 μl of dialyzed asolectin vesicles. After centrifugation for 30 min at 50,000 rpm the resulting pellet was resuspended, at 4°C, in ~150 μl of HEPES buffer containing 5% ethylene glycol (pH 7.4). Small drops of this suspension were deposited on microscope slides and submitted to partial dehydration at 4°C, for ~2 h in a refrigerator. The samples were rehydrated by addition of up to 30 μl distilled water on top of each dehydrated spot. Samples were rehydrated overnight at 4°C inside a petri dish containing a wet paper pad on the bottom. The resulting giant liposomes were pipetted off the rehydrated drops carefully and stored on ice.

### Patch-clamp recordings of ion channels

Giant liposome suspensions (20 μl) were added to a bath solution containing 150 mM Na-gluconate and 10 mM HEPES (pH = 7.4 with *N*′-methyl-D-glucamine (NMDG)) on a glass slide previously coated with poly-L-lysine and equilibrated for 2-3 h at room temperature. Single-channel currents were recorded using the patch-clamp technique (23) in inside-out configuration (similar results for cell-attached configuration) to control ionic conditions on both sides of the channels. In a sodium-free bath solution, Na-gluconate was substituted by 150 mM NMDG (pH = 7.4 with gluconic acid). An Ag/AgCl electrode in combination with a 3 M KCl-filled agar bridge was used as reference electrode. The stability of electrode potentials was carefully checked at the end of each experiment, excluding those with drift above +/− 3 mV. Soft glass pipettes immersed in bath solution exhibited a resistance of 4–6 M Ohms. Pipette solution contained 105 mM $MgCl_2$, $CaCl_2$, $MnCl_2$, $CoCl_2$ or $NiCl_2$ and 10 mM HEPES (pH = 7.4 with HCl). In pipette solution with a decreased/omitted $MgCl_2$ concentration, osmolarity was adjusted by including 150 mM NMDG. In some experiments 100 μM $LaCl_3$, or 1 mM Cobalt(III)-hexaammine (Co(III)-Hex) was included in the pipette solution or 100 μM of the $Cl^-$-channel blocker 5-nitro-2-(3-phenylpropylamino) benzoic acid (24) was added to the bath solution. The latter blocker did not affect single channel characteristics of Mrs2. Current signals were detected using a List-Medical EPC7 amplifier (Darmstadt, Germany), low pass filtered at 0.5 KHz and recorded as well as analyzed with Clampex 9.0 and Clampfit 9.0 from Axon Instruments (Foster City, CA). According to the electrophysiological conventions, potentials are given for the inside of vesicles, representing the mitochondrial matrix, relative to their outside. Hence, an influx of cations into vesicles is depicted as negative current. Applied potentials were corrected for a liquid junction of −15 mV resulting from a gluconic-acid-based bath solution and a $Cl^-$-based pipette solution. Single-channel amplitude and open probabilities were determined from amplitude histograms at each potential. Slope conductances were obtained by linear regression fit of current-voltage relationships and are presented as mean ± SE value. Single channel dwell times determined within 3-ms time windows were fit in a histogram with one (open dwell times) or two (closed dwell times) exponential decays for dwell times >1 ms and <800 ms.

### Laser confocal microscopy

Giant lipid vesicles fused with Mrs2-HA containing SMPs were attached to poly-L-lysine (Sigma-Aldrich) coated glass slides and treated with 0.1% Triton X-100 for 4 min in some cases ($n = 4$). Mrs2-HA was visualized with anti-HA antibody followed by Alexa 594-conjugated anti-mouse as the secondary antibody (Molecular Probes, Eugene, OR). Aac2p was stained with anti-Aac2 antibody followed by secondary Alexa 488 anti-rabbit antibody (Molecular Probes). Coverslips were mounted on glass slides using

an Anti-Fade kit (Molecular Probes). Confocal images were captured with a Zeiss LSM510 laser confocal microscope equipped with argon (488 nm) and krypton (594 nm) lasers and a 40× oil objective. Red, green, and differential interference contrast (DIC) channels were digitally pseudocolored using the LSM510 scanning control program and Image Browser v2.30.011 (Zeiss, Jena, Germany).

### Polyacrylamide gel electrophoresis and Western blot

Mitochondria were isolated from an *mrs2*Δ yeast strain expressing the MRS2-HA, MRS2-HA(Δ277–282), or MRS2-HA(ins207/208) construct from a multicopy vector. Mitochondrial preparations (30 $\mu$g) were mixed with loading buffer containing $\beta$-mercaptoethanol and samples were heated to 80°C for 4 min before loading on sodium dodecylsulfate–polyacrylamide gels. Mrs2-HA protein-containing bands were visualized by use of an HA antiserum.

## RESULTS

### Mrs2p forms a $Mg^{2+}$ permeable channel

To reveal the nature of $Mg^{2+}$ transport by Mrs2p we performed patch clamp electrophysiology on lipid giant vesicles (up to 200 $\mu$m in diameter) fused with inner-mitochondrial membranes originating from Mrs2p overexpressing yeast cells (Fig. 1 *A*). The mitochondria in the giant lipid vesicles reassumed a right-side-out orientation with the N- and C-terminal sequences of Mrs2p located within, and the short loop connecting the transmembrane domains outside of the vesicles (Fig. 1 *B*). Analysis of single channel characteristics enabled a detailed comparison whether the Mrs2p expressed from a multicopy vector (''overexpressed'') corresponded to channels expressed from the chromosomal MRS2 and LPE10 genes (''endogenous'').

Fig. 2 *A* shows representative consecutive current traces reflecting open and closed states of single overexpressed Mrs2p-derived channels. The pipette solution included 105 mM $MgCl_2$ and the bath solution contained 150 mM Na-gluconate. Currents were recorded throughout the study in the inside-out configuration at test potentials ranging from +5 to −45 mV. An increase in channel amplitudes correlated with an increase in negative potentials, consistent with $Mg^{2+}$ permeation through overexpressed Mrs2p channels and was strictly dependent on the presence of $Mg^{2+}$ in the pipette (see also next paragraphs on Mrs2p permeability and Cobalt(III)-hexaammine). A current-voltage relationship determined at negative potentials yielded a single channel conductance of 153 ± 2 pS (Fig. 2 *B*). The high Mrs2p conductance was obtained in nine out of 13 experiments, whereas no inward current could be detected in the remaining experiments indicating a high abundance of Mrs2p within these vesicles, and presuming that in only four out of 13 patches no Mrs2p channel was present. Outward single channel currents of various amplitudes were also observed at positive potentials (data not shown) suggesting the presence of further endogenous $Na^+$ or $Cl^-$ permeabilities.

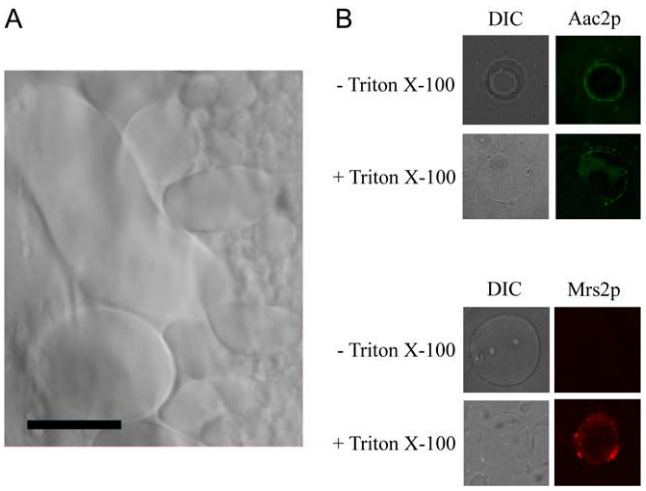


FIGURE 1 Characterization of reconstituted giant liposomes. Asolectin lipids were fused with mitochondrial inner membrane vesicles (6) isolated from cells expressing an Mrs2-HA fusion protein expressed from a YEp multicopy vector. (*A*) Transmitted image of giant lipid vesicles fused with inner mitochondrial membrane vesicles (630-fold enlargement with oil objective). Scale bar, 60 $\mu$m. (*B*) Orientation of Mrs2p in giant lipid vesicles. Vesicles were attached to poly-L-lysine coated glass slides and analyzed before or after treatment with Triton X-100 to partially dissolve membranes. (*Left panels*) Transmitted light images. (*Right panels*) Mrs2-HA visualized by use of anti-HA antibody followed by Alexa 594-conjugated anti-mouse as the secondary antibody, and Aac2p visualized with anti-Aac2 antibody followed by secondary Alexa 488 anti-rabbit antibody. The samples were viewed with a Zeiss LSM laser confocal microscope. The ADP/ATP carrier Aac2p exposes epitopes on the outside of the inner mitochondrial membrane whereas the Mrs2 C-terminus with the HA epitope is on the matrix side. Accordingly, Aac2 is accessible in both samples. The HA tag of Mrs2p, in contrast, was accessible after the vesicles had been ruptured. We conclude therefore that the vesicles have a right-side-out orientation.

When lipid vesicles containing endogenous mitochondrial membranes of wild-type yeast cells (single copy of *MRS2* and *LPE10* genes) were used, we recorded in five out of 23 experiments channel activity (Fig. 2 *C*) with a $Mg^{2+}$ conductance of 152 ± 3 pS (Fig. 2 *D*) similar to that of overexpressed Mrs2p. To further characterize and compare single channel properties of both overexpressed Mrs2p and endogenous Mrs2p channels we analyzed their open as well as closed dwell times and determined their open probabilities. Open dwell time at −25mV exhibited a monoexponential decay with a time constant $\tau$ of 16.3 ± 0.5 ms or 17.7 ± 0.7 ms for either endogenous or overexpressed Mrs2p, respectively (Fig. 2 *E*). Closed dwell times at −25mV were best fit by two exponentials resulting in a $\tau_{fast}$ of 3.8 ± 0.04 ms or 4.0 ± 0.05 ms and a $\tau_{slow}$ of 33.6 ± 3.6 ms or 32.8 ± 1.9 ms for endogenous or overexpressed Mrs2p, respectively (Fig. 2 *F*). Additionally, single channel open probability was calculated to ~60% for potentials ranging from −5 to −35 mV for either endogenous or overexpressed Mrs2p (Fig. 2 *G*).

The similarity in conductance, open probability, as well as open and closed dwell times of single channels from

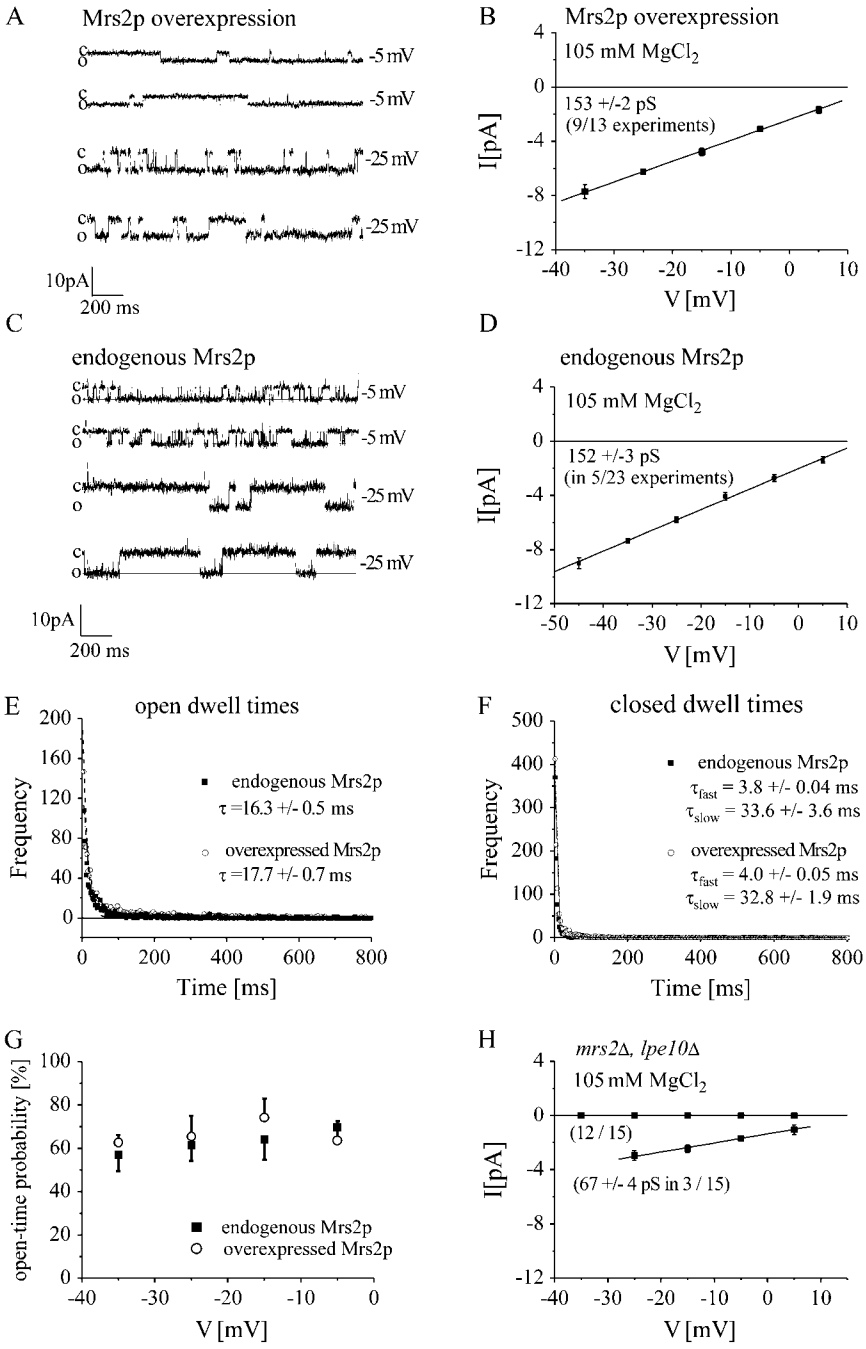


FIGURE 2 Single-channel currents mediated by overexpressed or endogenous Mrs2p channels. Single-channel currents were obtained in inside-out configuration from reconstituted giant vesicles fused with inner mitochondrial membrane particles. (*A*) Recordings of vesicles with Mrs2p overexpressed from a multicopy plasmid in *mrs2*Δ, *lpe10*Δ genetic background. $Mg^{2+}$ (105 mM) was used as a charge carrier and currents were recorded at −5 mV and −25 mV. (*C*) Similar single-channel activity was recorded at −5 mV and −25 mV from lipid vesicles containing mitochondrial membranes of wild-type yeast cells. (*B* and *D*) Current-voltage relationships were determined by use of single-channel currents determined from amplitude histograms at indicated potentials and yielded single-channel conductances of 153 ± 2 pS for vesicles with overexpressed Mrs2p (*B*) or 152 ± 3 pS with endogenous Mrs2p (*D*). (*E* and *F*) Open dwell times (*E*) or closed dwell times (*F*) histograms for either endogenous or overexpressed Mrs2p. Open dwell times were fit with a mono-exponential decay (endogenous Mrs2, $\tau = 16.3 \pm 0.5$ ms; overexpressed Mrs2, 17.7 ± 0.7 ms), whereas closed dwell times were fitted with a biexponential decay (endogenous Mrs2, $\tau_{fast} = 3.8 \pm 0.04$ ms; $\tau_{slow} = 33.6 \pm 3.6$ ms; overexpressed Mrs2, $\tau_{fast} = 4.0 \pm 0.05$ ms; $\tau_{slow} = 32.8 \pm 1.9$ ms). (*G*) Open probabilities for either overexpressed or endogenous Mrs2p channels are calculated between potentials of −5 mV to −35 mV. (*H*) Current-voltage relationship of single-channel currents between a potential of +5 mV to −25 mV yielded a conductance of 67 ± 4 pS for vesicles lacking Mrs2-type proteins (*mrs2*Δ, *lpe10*Δ) based on three out of 15 experiments with no significant conductances in the remaining 12 experiments.

overexpressed and endogenous Mrs2p suggested an identical molecular origin.

As a control, *MRS2* and its close homolog *LPE10* were deleted (*mrs2*Δ, *lpe10*Δ), and vesicles prepared from these yeast mitochondria were recorded under identical conditions (Fig. 2 *H*). Here we observed either no inward currents (12 out of 15 experiments) or a channel with a smaller conductance of 67 ± 4 pS (three out of 15 experiments). This channel activity with a conductance of ~65 pS was generally observed with the 105 mM $Mg^{2+}$-containing solution at a probability of ~15%, but was excluded from further analysis due to its unknown molecular identity. These data led us to conclude: i), that the 155 pS $Mg^{2+}$ conductance resulted from the activity of the Mrs2 protein, and ii), that yeast mitochondria have a second channel activity of lower conductance of unknown origin.

## Permeability of the Mrs2p channel

The above-mentioned existence of endogenous $Na^+$ or $Cl^-$ single channel conductance rendered it difficult to determine the reversal potential for Mrs2p activity recorded

with 105 mM $MgCl_2$. Therefore standard bath solution containing 150 mM Na-gluconate was substituted by 150 mM NMDG-gluconate that enabled to resolve Mrs2p activity up to +35 mV. In line with data of Fig. 2, current-voltage relationship between a potential of −35 to +5 mV was linear, yielding 157 ± 1 pS in six out of eight experiments for overexpressed Mrs2p channels. For potentials of +15 mV to +35 mV the I/V relationship showed asymptotic convergence to the *x* axis, extrapolating to a reversal potential of >+40 mV (Fig. 3 *A*), consistent with Nernst equation for a $Mg^{2+}$ selective ion channel. Vesicles lacking Mrs2-type channel proteins did not lead to detectable conductances in seven out of 10 experiments and showed a reduced conductance in three experiments (50 pS, $n = 1$ and 10 pS, $n = 2$; Fig. 3 *A*).

We additionally tested if the Mrs2p channel is permeable to other divalent cations ($Ca^{2+}$, $Mn^{2+}$, $Co^{2+}$, $Ni^{2+}$). Initial control experiments with 105 mM $Ca^{2+}$ in the pipette and vesicles lacking Mrs2p and Lpe10p revealed single channel activity of large amplitudes (data not shown) suggesting that yeast mitochondria most likely have endogenous $Ca^{2+}$ permeable channels. To inhibit activities of these endogenous $Ca^{2+}$ permeable channels, $LaCl_3$ (100 $\mu$M) was used. With $LaCl_3$ (100 $\mu$M) added to the 105 mM $CaCl_2$ pipette solution, single channel conductances, recorded from *mrs2*Δ, *lpe10*Δ vesicles, did not exceed values of 7 pS that were in a similar range as observed with vesicles overexpressing Mrs2p (Fig. 3 *B*). This lack of $Ca^{2+}$ permeation through Mrs2p channels was, however, not due to their inhibition by $LaCl_3$. Mrs2p-mediated $Mg^{2+}$ currents with a reduced single channel conductance were clearly detected (97 ± 8 pS in five out of five experiments) when $LaCl_3$ was added to 105 mM $MgCl_2$ pipette solution (data not shown). The decrease in single channel conductance suggests a weak, rapid block of the $Mg^{2+}$ permeation pathway of Mrs2 by $La^{3+}$. In the following, pipette solution was exchanged to either 105 mM $MnCl_2$ (Fig. 3 *C*), 105 mM $CoCl_2$ (Fig. 3 *D*), or 105 mM $NiCl_2$ (Fig. 3, *E* and *F*). Current-voltage relationships revealed small background conductances without significant difference between vesicles with Mrs2p overexpressed and vesicles lacking Mrs2-type channels with either a $Mn^{2+}$- (Fig. 3 *C*) or $Co^{2+}$-containing pipette solution (Fig. 3 *D*). In contrast, 105 mM $Ni^{2+}$ resulted in a 43 ± 5 pS conductance between −35 and −5 mV visible only in Mrs2p overexpressing vesicles (five out of eight experiments), whereas background single-channel conductances (<7 pS) in either Mrs2p overexpressing or knock-out vesicles were not significantly different (Fig. 3 *E*). Representative single channel $Ni^{2+}$ currents through Mrs2p are shown at a potential of −25 mV (Fig. 3 *F*).

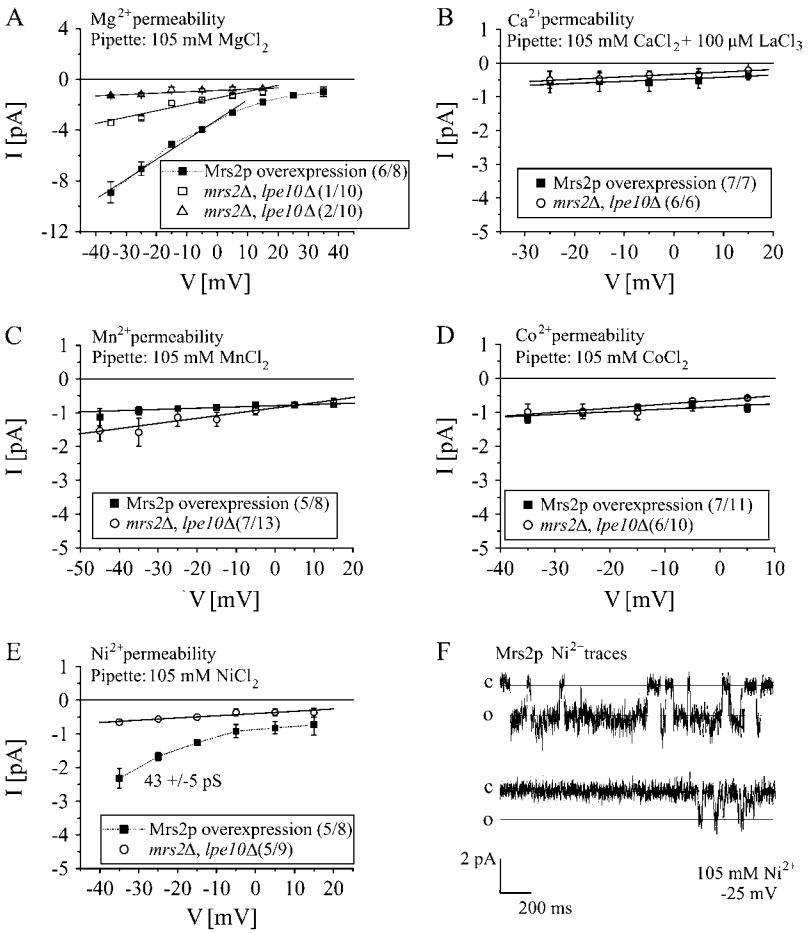


FIGURE 3 Permeability of Mrs2p channel. (*A*) Single channel recordings were measured with a pipette solution containing 105 mM $MgCl_2$ and a bath solution including 150 mM NMDG and gluconic acid. Current-voltage relationships between +35 mV and −35 mV of single overexpressed Mrs2p channels yielded a conductance of 157 ± 1 pS in six out of eight experiments, whereas control vesicles lacking Mrs2-type channel proteins (*mrs2*Δ, *lpe10*Δ) led to a reduced conductance of 50 pS in 1/10 experiments and 10 pS in 2/10 experiments and lacked single channel activities in 7/10 experiments. (*B–D*) Single-channel current-voltage relationships recorded from Mrs2p overexpressing vesicles and control vesicles lacking Mrs2-type channel proteins were not significantly different with either a pipette solution of 105 mM $CaCl_2$ + 100 $\mu$M $LaCl_3$ (*B*), 105 mM $MnCl_2$ (*C*), or 105 mM $CoCl_2$ and the bath solution as described in panel *A*. (*E*) Current voltage relationship from single channel recordings showed a $Ni^{2+}$ conductance of 43 ± 5 pS in five out of eight experiments only in Mrs2p overexpressing vesicles. Additionally, smaller conductances of similar ranges were observed in both Mrs2p overexpressing (not shown) or Mrs2 lacking vesicles. (*F*) Single-channel current traces were recorded at a test potential of −25 mV with 105 mM $NiCl_2$ from vesicles with overexpressed Mrs2p.

These data suggest that Mrs2p channels are mainly permeable for $Mg^{2+}$, with an ~3.5-fold smaller $Ni^{2+}$ permeability. However, no Mrs2p-mediated currents could be observed for either $Ca^{2+}$, $Mn^{2+}$, or $Co^{2+}$.

## Cobalt(III)-hexaammine inhibits Mrs2p channels

We and others have previously shown that cobalt-hexaammine (Co(III)-Hex), an analog for the hydrated $Mg^{2+}$ ion, markedly blocks $Mg^{2+}$ entry through Mrs2p in Fura-2 experiments (7) as well as CorA-mediated $Mg^{2+}$ uptake in bacteria (25).

Therefore, to examine for its inhibitory effect on Mrs2 channels, 1 mM Co(III)-Hex was included in the 105 mM $MgCl_2$ pipette solution. Current traces clearly revealed a reduction of single-channel amplitudes in the presence of 1 mM Co(III)-Hex corresponding to a conductance of 33 ± 3 pS in six out of eight experiments (Fig. 4 *B*). The full 155-pS conductance was never observed in the presence of Co(III)-Hex (Fig. 4 *A*). Additionally, not only the amplitude of single Mrs2p channels was affected by Co(III)-Hex but also the open-time probability decreased to ~30% (Fig. 4 *C*). The closed dwell time could be best fit with a single exponential $\tau$ of 13.3 ± 0.35 ms (data not shown). For a better comparison with our previous mag-fura2 experiments carried out with 10 mM $Mg^{2+}$ (7), we then used an analogous pipette solution containing also 10 mM $MgCl_2$ and 150 mM NMDG. Mrs2p overexpressing vesicles revealed channels with a conductance of 111 ± 4 pS in seven out of eight experiments (Fig. 4 *D*). When 1 mM Co(III)-Hex was included, these Mrs2p showed a substantially reduced conductance of 20 ± 2 pS (four out of seven experiments; Fig. 4 *D*). These single-channel amplitudes were, however, not significantly different to those recorded from vesicles lacking Mrs2-type channels in a 10 mM $MgCl_2$ pipette solution without Co(III)-Hex (Fig. 4 *D*). Similarly small background conductances were also observed in both Mrs2p and Mrs2-type knock-out vesicles with a pipette solution including only 150 mM NMDG (data not shown). These data are in line with the previous mag-fura2 measurements (7) where $Mg^{2+}$ uptake in the presence of Co(III)-Hex has been abolished down to levels of Mrs2-knockout mitochondria.

## $E_{341}K$, $E_{342}K$ substitutions in the loop region of Mrs2p abolish conductance

The short loop between the two transmembrane domains of most CorA, Mrs2, and Alr1 proteins contains one or two negatively charged residues that may contribute to electrostatic attraction of $Mg^{2+}$ to the outer side of the pore (4,8, 9,14,26). Yeast Mrs2 and mammalian Mrs2 proteins contain two glutamates (E341, E342) in this loop. Although their substitution by two aspartates (Mrs2-J10: $E_{341}D$, $E_{342}D$) in yeast Mrs2p had no apparent negative effect, their substitution by two lysines (Mrs2-J11: $E_{341}K$, $E_{342}K$) abolished both complementation of the *mrs2*Δ growth defect as well as $Mg^{2+}$ influx as analyzed by mag-fura2 (26). We overexpressed these mutant proteins Mrs2-J10 ($E_{341}D$, $E_{342}D$) and Mrs2-J11 ($E_{341}K$, $E_{342}K$) and recorded single-channel currents in the standard pipette solution of 105 mM $MgCl_2$. Single-channel amplitudes of Mrs2-J10 that carried the conservative mutations yielded a conductance of 156 ± 1 pS in a total of five experiments (Fig. 5 *A*) similar to wild-type Mrs2. Representative single-channel traces were shown for Mrs2-J10 recorded at potentials of −5 mV and −25 mV (Fig. 5 *C*). The amplitude histogram revealed one clear open state determined for −25 mV with an amplitude of ~6 pA

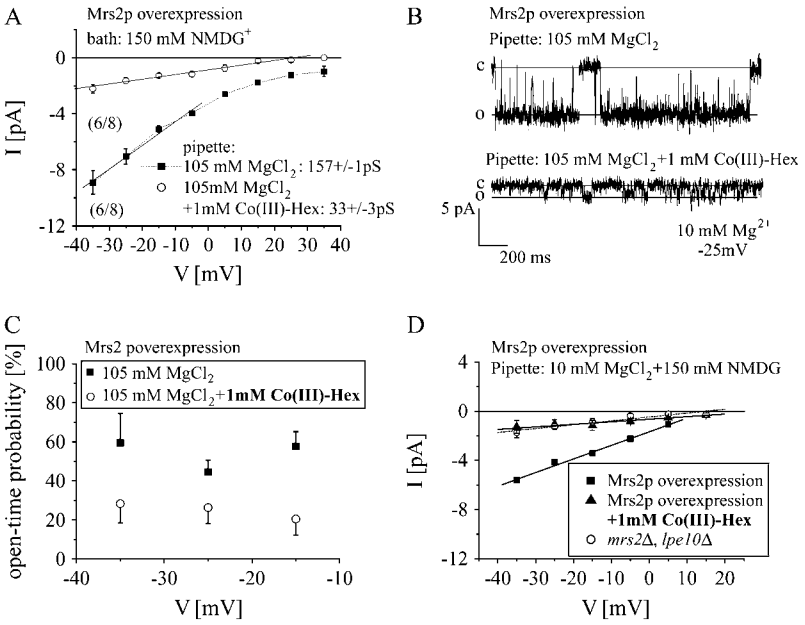


FIGURE 4 Mrs2p currents were inhibited by Co(III)-Hex. (*A*) Current-voltage relationships of overexpressed Mrs2p with a pipette solution of 105 mM $MgCl_2$ and a bath solution including 150 mM NMDG yielded single-channel conductances of 157 ± 1 pS (six out of eight experiments) in the absence and of 33 ± 3 pS (six out of eight experiments) in the presence of 1 mM Co(III)-Hex. (*B*) Single-channel current traces from overexpressing Mrs2p vesicles were recorded at a test potential of −25 mV with a pipette solution of 105 mM $MgCl_2$ with or without 1 mM Co(III)-Hex. (*C*) Open probabilities of overexpressed Mrs2p channels were calculated between potentials of −15 mV to −35 mV for a pipette solution including 105 mM $MgCl_2$ with or without 1 mM Co(III)-Hex. (*D*) Current-voltage relationship of overexpressed Mrs2p with a pipette solution of 10 mM $MgCl_2$ and 150 mM NMDG and a bath solution including 150 mM NMDG yielded single-channel conductances of 111 ± 4 pS (seven out of eight experiments). Addition of 1 mM Co(III)-Hex (four out of seven experiments) inhibited Mrs2p channel activity to similarly small current amplitudes as observed from control vesicles lacking Mrs2 (six out of 11 experiments).

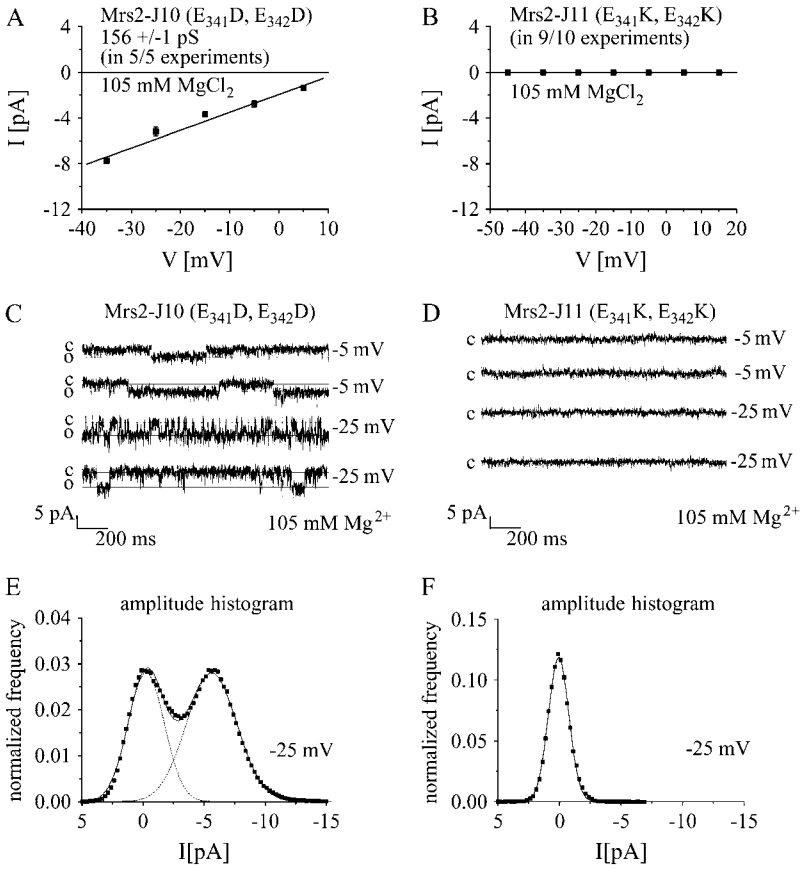


FIGURE 5 Negatively charged amino acids in the loop of Mrs2p are essential for $Mg^{2+}$ conductances. A schematic drawing depicting point mutations of Mrs2p in the intermembrane space, where two glutamic acids at position 341, 342 were either changed to aspartic acids (Mrs2-J10) or lysines (Mrs2-J11) (26). (*A* and *B*) Current-voltage characteristics of single Mrs2-J10 channels yielded a conductance of 156 ± 1 pS with 105 mM $Mg^{2+}$ (five out of five experiments), whereas no $Mg^{2+}$ conductance was observed from vesicles with Mrs2-J11 overexpressed from a multicopy plasmid in an *mrs2*Δ genetic background in nine out of 10 experiments. (*C* and *D*) Single-channel traces are shown for overexpressed Mrs2-J10 (*C*) or Mrs2-J11 (*D*) at potentials of −5mV and −25mV. (*E* and *F*) Amplitude histograms at a potential of −25 mV determined from single-channel traces of overexpressed Mrs2-J10 (*E*) and Mrs2-J11 (*F*).

and an open probability of 51 ± 13% (Fig. 5 *E*) that was not significantly different to that of overexpressed wild-type Mrs2p channels.

In a similar approach we recorded overexpressed Mrs2-J11 (nonconservative mutations ($E_{341}$K, $E_{342}$K) with standard pipette solution of 105 mM $MgCl_2$. However, the mutations of glutamic acids to lysines seemed to be critical for Mrs2p channels as we failed to detect $Mg^{2+}$ conductances in nine out of 10 experiments as evident from the current-voltage relationship (Fig. 5 *B*), single-channel traces (Fig. 5 *D*), and from the amplitude histogram (Fig. 5 *F*). The remaining experiment showed a similarly small conductance as observed in *mrs2*Δ, *lpe10*Δ mitochondria (cf. Fig. 2 *H*). These results support the notion that negatively charged residues might be relevant for the attraction of $Mg^{2+}$ to the pore (4,8,9,14,26). Yet a negative effect of the $E_{341}$K, $E_{342}$K substitution on folding structures of the loop sequence is not excluded.

## Mrs2p coiled-coil mutations resulted in elevated $Mg^{2+}$ influx into mitochondria

Computational analyses of Mrs2 proteins performed before structures of any related protein were available revealed coiled-coil motifs in helical regions N-terminal to the TM domains (Supplementary Fig. S1B). We generated an insertion (Mrs2-HA(ins207/208)), which increased the predicted probability for a coiled-coil domain, and a deletion (Mrs2-HA(Δ277–282)), which drastically decreased it as calculated by the COILS program (Supplementary Fig. S1B). When the molecular structure of *Thermotoga maritima* CorA became available (4), we tentatively identified the sequences affected by these mutations as the end of helix α5 and the beginning of helix 7 (Supplementary Fig. S1A). In the crystal structure of CorA the helices α5–α7 form an ''elbow'' structure that has been proposed to transmit signals from the α/β-fold at the $Mg^{2+}$ binding N-terminus to the membrane pore (4,8,9).

To observe effects of mutations Mrs2-HA(ins207/208) and Mrs2-HA(Δ277–282) on Mrs2p oligomerization (7) we used blue-native polyacrylamide gel electrophoresis (BN-PAGE) (20,27) followed by immunoblotting to detect Mrs2 proteins with either a myc or an HA epitope tag at their C-termini (Fig. 6 *C*). When the wild-type versions were expressed, a single product band of high molecular weight of ~470 kDa (Mrs2-myc; Fig. 6 *C*) or of 270 kDa (Mrs2-HA; Fig. 6 *C*) was detected.

BN-PAGE with mitochondria expressing the Mrs2-HA(Δ277–282) and Mrs2-HA(ins207/208) mutant proteins yielded a product of an apparent molecular weight of ~270 kDa, but in addition bands of 150–200 kDa and of ~70 kDa, probably representing Mrs2-containing complexes of intermediary size and the monomer, respectively (Fig. 6 *C*, *right*

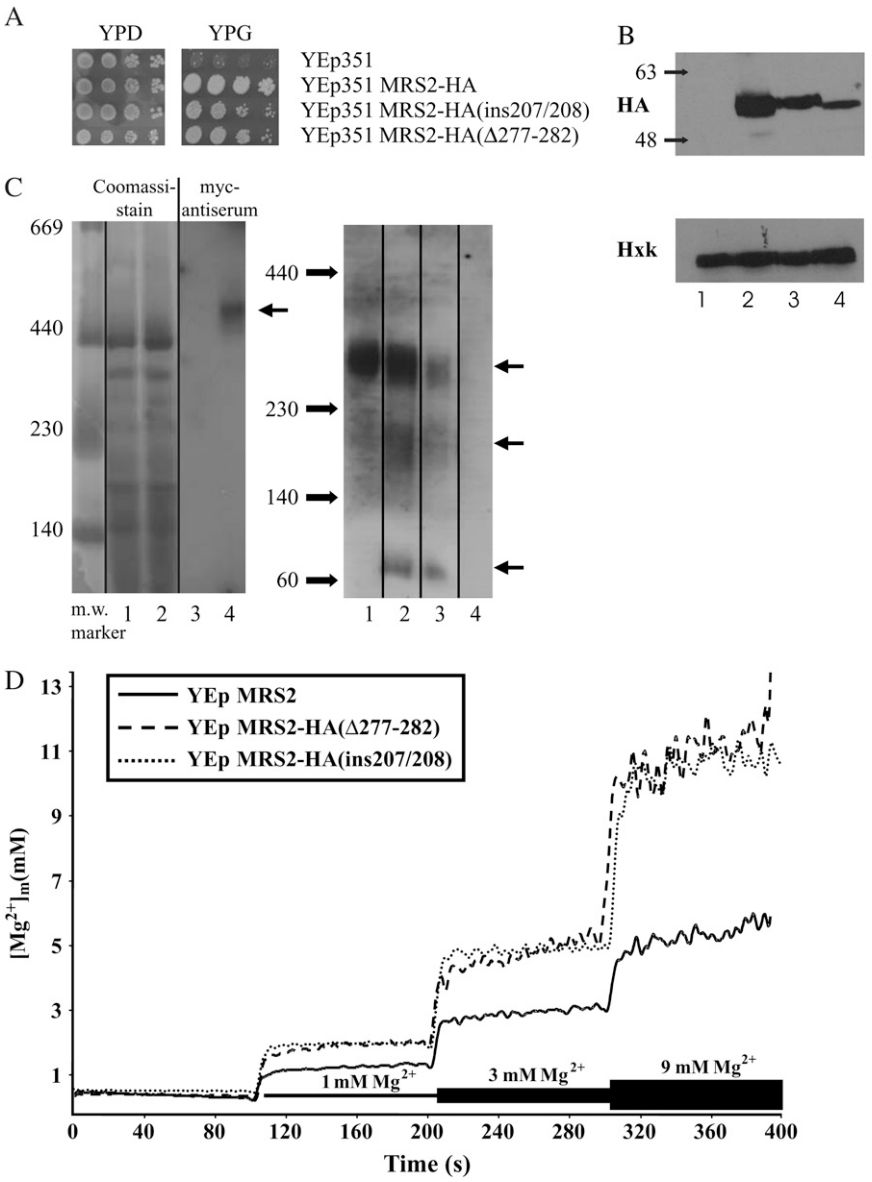


FIGURE 6 Coiled-coil mutations affect stability of Mrs2p channel complex as well as its $Mg^{2+}$ uptake. (*A*) Partial complementation of the *mrs2*Δ growth defect by the expression of two coiled-coil mutants *Mrs2*-HA(ins207/208) and *Mrs2*-HA(Δ277–282) from a high copy number plasmid. Mutant *mrs2*Δ cells were transformed with the empty plasmid YEp351, with this plasmid containing the wild-type MRS2-HA construct or the MRS2-HA(ins207/208) or MRS2-HA(Δ277–282) mutant constructs. Serial dilutions of the indicated strains were used to inoculate agar plates, which then were grown for 4 days (*YPD*) or 6 days (*YPG*) at 28°C. (*Left panel*) Growth on fermentable substrate (*YPD*); (*right panel*) growth on nonfermentable substrate (*YPG*). (*B*) Expression of Mrs2-HA products. Mitochondrial proteins of *mrs2*Δ mutant cells transformed with the empty YEp351 multicopy plasmid (lane *1*) or the same plasmid expressing Mrs2-HA (lane *2*), MRS2-HA(ins207/208) (lane *3*) or MRS2-HA(Δ277–282) (lane *4*) were separated by PAGE and Mrs2-HA proteins were made visible by immunoblotting involving an HA antiserum. (Calculated masses of these proteins are 54.2 kDa for Mrs2-HA, 55 kDa for MRS2-HA(ins207/208), and 53.4 kDa for MRS2-HA(Δ277–282) proteins). As a loading control hexokinase was detected by use of a polyclonal Hxk serum. (*C*) Mrs2p-containing complexes detected by blue-native gel electrophoresis. (*Left*) Mitochondria of *mrs2*Δ mutant mitochondria transformed with YEp112 (empty plasmid) and YEp112 MRS2-myc (lanes *1*, *3* and *2*, *4*, respectively) were isolated, proteins were solubilized in 1% laurylmaltoside. Lanes 1 and 2 visualize the Coomassie stained major mitochondrial protein complexes of the two samples; lane 3 and 4 represent the result of the immunoblotting with a myc antiserum. (*Right*) Mitochondria of *mrs2*Δ mutant mitochondria transformed with YEp351 MRS2-HA (lane *1*), YEp351 MRS2-HA(ins207/208), YEp351 MRS2-HA(Δ277–282) (lanes *2* and *3*, respectively) and YEp351 empty plasmid (lane *4*) were isolated, proteins were solubilized in laurylmaltoside (1%) and submitted to BN-PAGE. Gels were analyzed by immunoblotting with an HA antiserum. Molecular weights of Mrs2-myc and Mrs2-HA monomers (without their mitochondrial targeting sequences (36) were calculated to be 70 and 55 kDa, respectively. (*D*) $[Mg^{2+}]_e$-dependent changes of $[Mg^{2+}]_m$ in wild-type and coiled-coil mutant mitochondria. Mitochondria were isolated from cells expressing either wild-type Mrs2p or the coiled-coil mutant versions Mrs2-HA(Δ277–282) of Mrs2-HA(ins207/208) from a multicopy vector (YEp351) in an *mrs2*Δ yeast strain, loaded with the $Mg^{2+}$ sensitive fluorescent dye mag-fura 2. Intramitochondrial free $Mg^{2+}$ concentrations ($[Mg^{2+}]_m$) were determined in nominally $Mg^{2+}$ free buffer or upon addition of $Mg^{2+}$ to external $Mg^{2+}$ concentrations $[Mg^{2+}]_e$ as indicated in the figure.

*panel*, *lanes 2* and *3*). This approach clearly indicated that each of the two mutations in predicted coiled-coil motifs of Mrs2p affected either the assembly or lowered the stability of the Mrs2-containing complex.

Mutant Mrs2-HA(ins207/208) as well as Mrs2-HA(Δ277–282) proteins expressed as C-terminal fusions with an HA tag from a high copy number plasmid (YEp351) restored growth of *mrs2*Δ mutant cells on nonfermentable substrate (Fig. 6 *A*) although they were expressed at lower levels than the wild-type Mrs2 protein (Fig. 6 *B*).

Additionally, we used the mag-fura 2 $Mg^{2+}$-sensitive dye entrapped in isolated mitochondria to determine changes in matrix free ionized $Mg^{2+}$ ($[Mg^{2+}]_m$) (7). *Mrs2*Δ mutant mitochondria with Mrs2-HA(Δ277–282) or Mrs2-HA(ins207/208) expressed from a high copy number vector exhibited initial rates of increase in $[Mg^{2+}]_m$ with $[Mg^{2+}]_e$ of 1, 3, or 9 mM similar for both coiled-coil mutants and wild-type Mrs2p when expressed from the same vector. However, influx proceeded for extended time periods resulting in steady-state $Mg^{2+}$ plateau levels increased by ~55% at 1 mM $[Mg^{2+}]_e$, ~60% at 3 mM $[Mg^{2+}]_e$, and ~140% at 9 mM $[Mg^{2+}]_e$, to add up to ~11 mM $[Mg^{2+}]_m$ (Fig. 6 *D*). This is at variance with our previous findings that overexpression of wild-type Mrs2p significantly increases influx rates, but not steady-state

$[Mg^{2+}]_m$ (7). It appears thus that the coiled-coil mutations affected the $Mg^{2+}$ homeostasis control, possibly by increasing the time of $Mg^{2+}$ influx into mitochondria. It remains to be shown whether this effect is mediated by reduced Mrs2 oligomer stability (as indicated by the BN analyses) or rather by changes of the $\alpha$5–$\alpha$7 fold of individual Mrs2 proteins, or by both.

## Mutations in coiled-coil domains of Mrs2p alter single-channel conductance

Single-channel currents from Mrs2-HA(Δ277–282) or Mrs2-HA(ins207/208) overexpressing mitochondria were recorded with a standard pipette solution of 105 mM $MgCl_2$ (Fig. 7). Although Mrs2-HA(Δ277–282) mutants behaved similarly to the wild-type channel in three out of 10 experiments (data not shown), we more frequently observed a number of substates in the remaining experiments as exemplarily shown for at a potential of either −5 mV (Fig. 7 *B*) or −25 mV (Fig. 7 *E*) in contrast to wild-type Mrs2p (Fig. 7, *A* and *D*). Similarly, overexpression of Mrs2-HA(ins207/208) yielded activity with a frequent occurrence of substates in comparison to wild-type Mrs2p in three out of five experiments recorded at a potential of −5 mV (Fig. 7 *C*) or −25 mV (Fig. 7 *F*). A typical Mrs2p conductance was also observed in two out of five experiments (data not shown).

To evaluate the functional effects of the coiled-coil mutants on a longer timescale, we determined single-channel amplitude histograms (Fig. 7, *G–I*). This revealed two characteristics that are affected when the probability of coil-

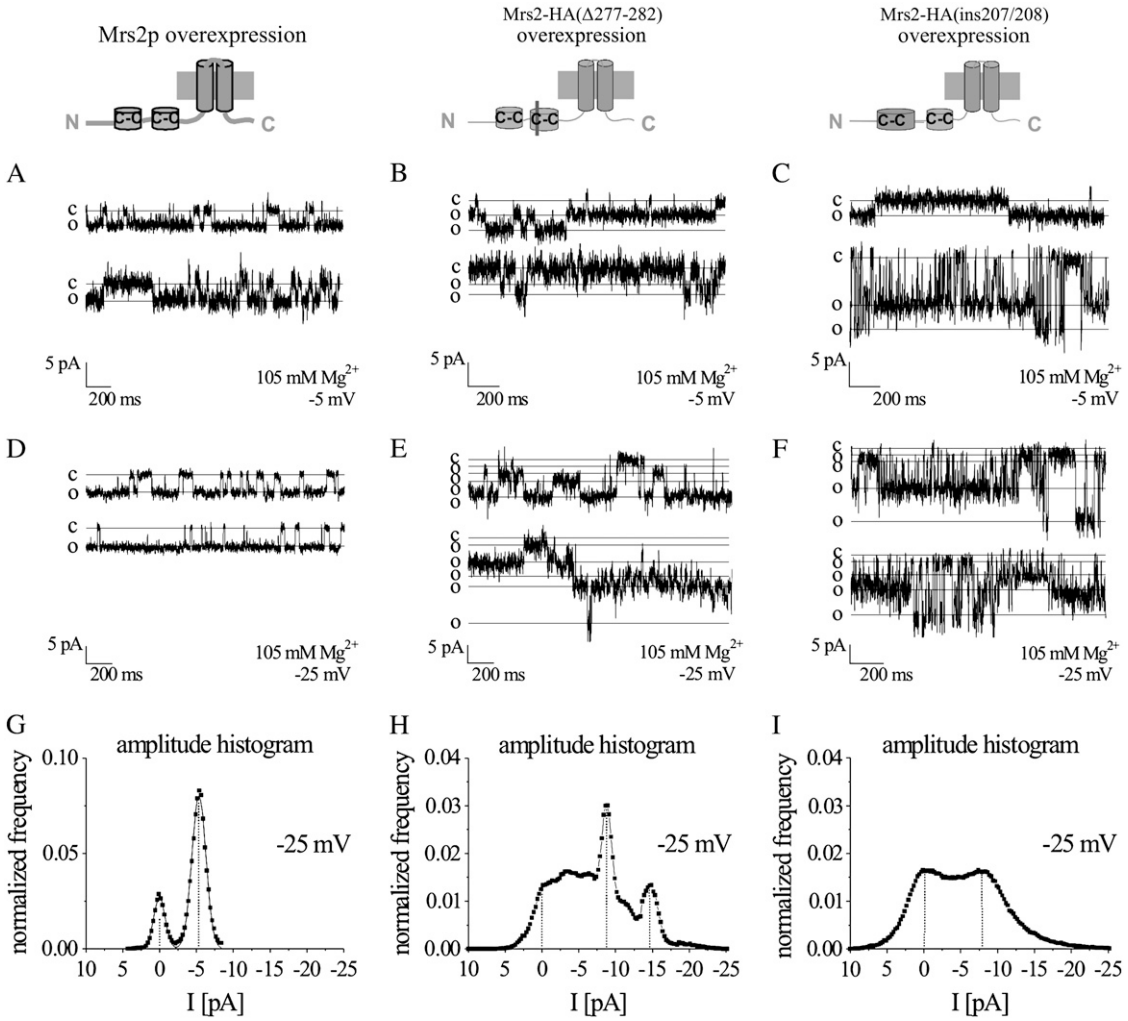


FIGURE 7 Mutations in coiled-coil domains affect Mrs2p single-channel currents. A schematic drawing compares wild-type Mrs2p (*left*) with two Mrs2p mutants that contained either a deletion of the second coiled-coil domain (Mrs2-HA(Δ277–282); *middle*) or an insertion in the first coiled-coil region (Mrs2-HA(ins207/208); *right*). Coiled-coil domains were marked as C-C. (*A–F*) Single-channel current traces were recorded at a test potential of −5 mV (*B* and *C*) or −25 mV (*D* and *E*) from vesicles with either wild-type *MRS*2 (*A* and *D*), *MRS2*-HA(Δ277–282) (*B* and *E*) or *Mrs2*-HA(ins207/208) (*C* and *F*) overexpressed from a multicopy plasmid in an *mrs2*Δ genetic background. (*G–I*) Representative amplitude histograms are depicted for the presented single-channel experiments determined over a period of ~160 s at a potential of −25 mV for either *MRS2* (*G*), *MRS2*-HA(Δ277–282) (*H*) and *MRS2*-HA(ins207/208) (*I*).

coiled formation is either reduced (Mrs2-HA(Δ277–282)) or increased (Mrs2-HA(ins207/208)). First of all, for both mutants a substantial broadening of the amplitude in the open states was evident reflecting the occurrence of multiple substates. Both the number of substates as well as their amplitudes showed high variation. Second, this broadening resulted in an increase in average open channel current. These electrophysiological results are consistent with those from magfura2 measurements, which revealed a significantly increased $Mg^{2+}$ influx upon multicopy expression of Mrs2-HA(ins207/208) or Mrs2-HA(Δ277–282) in comparison to wild-type Mrs2p (Fig. 6 *D*).

### Matrix $Mg^{2+}$ affects gating of the Mrs2p channel

Crystal structure of the CorA protein demonstrated that $Mg^{2+}$ ions can directly bind to the N-terminal domain, suggesting that these bound $Mg^{2+}$ ions may directly lead to a conformational reorientation of the N-terminal domain resulting in closing of the channel (4,8,9). Studies on $Mg^{2+}$ uptake by isolated mitochondria have also led to speculations that matrix $Mg^{2+}$ concentrations might control Mrs2p transport activity (7). We therefore examined on Mrs2p channel activity the effect of 1 mM $Mg^{2+}$ included to the bath solution of 150 mM NMDG. This increase in $Mg^{2+}$ concentrations from nominally free to 1 mM resulted in a shift of the current-voltage relationship to more negative potentials as expected from the reduction in driving force, yielding a reversal potential of +20 mV (five out of six experiments; Fig. 8 *A*). More importantly, open-time probability was significantly reduced from ~52% in the absence of $Mg^{2+}$ to ~20% in the presence of 1 mM $Mg^{2+}$ (Fig. 8 *B*). Representative current traces for Mrs2p channels including 1 mM $Mg^{2+}$ in the bath solution were shown for a test potential of −25 mV (Fig. 8 *C*).

These data represent strong experimental evidence that Mrs2 channels are not only able to sense matrix $Mg^{2+}$ concentrations but can additionally control $Mg^{2+}$ influx by an intrinsic feedback mechanism, as predicted from crystallographic analysis of CorA channel (4,8,9).

## DISCUSSION

Secondary structures of eukaryotic Mrs2 and Alr1 proteins align well with the core of a recently published bacterial CorA $Mg^{2+}$ transporter of *Thermotoga maritima,* supporting the notion of a CorA-Mrs2-Alr1 superfamily of ubiquitous $Mg^{2+}$ transport proteins (4). Yet it remained completely unclear whether its members act as cation transporters, or cation channels. Single-channel patch-clamp data presented here clearly revealed that one of the best characterized and representative members of the CorA related proteins, the yeast mitochondria Mrs2p, forms a $Mg^{2+}$-selective channel of high conductance.

As an alternative to whole mitoplast patch clamping (28–30), the use of lipid vesicles fused with submitochondrial particles expressing Mrs2p at a high level enabled us to resolve single Mrs2p channels. The occurrence of channels with $Mg^{2+}$ conductance of 155 pS correlated with the expression level of Mrs2p, whereas no channels of this conductance were observed in vesicles prepared from *mrs2*Δ, *lpe10*Δ knock-out mutants. A channel with lower conductance (~65 pS) was observed independent of the expression of Mrs2p. Its molecular identity remains to be determined.

The reversal potential of the Mrs2p channel was >+40 mV as expected for a $Mg^{2+}$ selective channel. With a 3.5-fold smaller conductance (~45 pS) Mrs2p also conducted $Ni^{2+}$ whereas it neither permeated $Ca^{2+}$, nor $Mn^{2+}$ or $Co^{2+}$. Permeability profile of the Mrs2 channel followed the size of dehydrated divalent ions with $Mg^{2+}$ radius (0.65 Å) < $Ni^{2+}$ (0.72 Å) < $Co^{2+}$ (0.74 Å) < $Mn^{2+}$ (0.8 Å) < $Ca^{2+}$ (0.99 Å). Yet it does not explain the substantial difference between $Ni^{2+}$ and $Co^{2+}$ that show a relatively similar radius. Thus, the hydration shell might impose further constraints for the

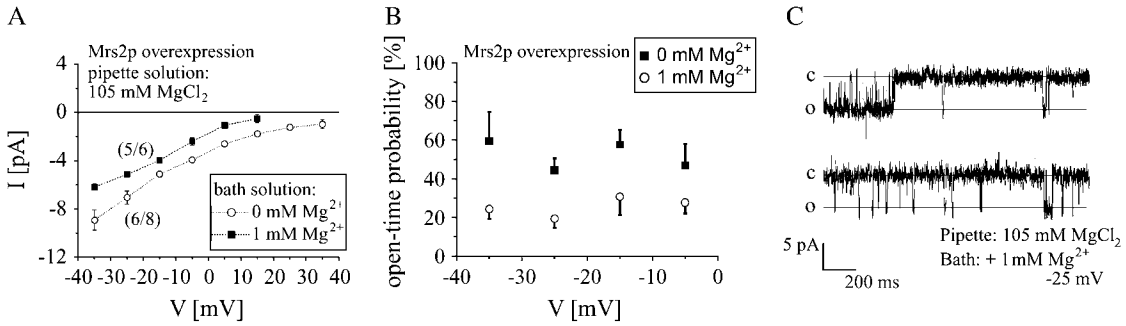


FIGURE 8 Matrix $Mg^{2+}$ decreases open probability of Mrs2p channels. (*A*) Current-voltage relationships of overexpressed Mrs2p with a pipette solution of 105 mM $MgCl_2$ shifted to more negative potentials when 1 mM $Mg^{2+}$ was included in the NMDG containing bath solution. (*B*) Open probabilities of overexpressed Mrs2p channels in the absence or presence of 1 mM $Mg^{2+}$ added to the bath solution were calculated between potentials of −5 mV to −35 mV. (*C*) Single-channel current traces were recorded from vesicles with overexpressed Mrs2p at a test potential of −25 mV with a pipette solution of 105 mM $MgCl_2$ and a bath solution of 150 mM NMDG with or without 1 mM $Mg^{2+}$ added to the bath solution.

transport through Mrs2 (9). We additionally observed suppression of $Mg^{2+}$ currents with a mixture of $Mg^{2+}/Co^{2+}$ (10/95 mM) in the pipette suggesting $Co^{2+}$ interaction probably with the pore (data not shown). CorA of *S. typhimurium* and Alr1 of yeast have been reported to transport $Ni^{2+}$ as well as $Co^{2+}$ (1,5). It remains to be seen if the lack of $Co^{2+}$ permeation by Mrs2p generally applies to Mrs2-type proteins.

The mammalian TRPM7 channel localized in the plasma membrane has been found to be permeable for all these divalent cations with a $Mg^{2+}$ conductance of 40 pS (10,31,32). Mrs2p and TRPM7 appear to be the major $Mg^{2+}$ permeable channels in their respective membranes, however, their protein structures seem to be completely different.

When applied to the outer side of the Mrs2p channel, Cobalt(III)-Hexaammine (Co(III)-Hex) was found to efficiently lower open-time probability concomitant to a reduction in single channel $Mg^{2+}$conductance. It had previously been shown to inhibit $Mg^{2+}$ uptake into bacteria, mitochondria or yeast cells mediated by CorA, Mrs2, or Alr1, respectively (5,25) (A. Graschopf, unpublished data). This supports the assumption of a common mechanism of $Mg^{2+}$ transport for CorA homologs and of an inhibitory action of Co(III)-Hex at the entrance or/and within the pore of the channels.

The entrance side of the channel pore is constituted by the short loop sequence connecting TM-A and TM-B with the GMN motif at the end of TM-A and negatively charged residues near TM-B, with a potential role in electrostatic attraction of $Mg^{2+}$ (4,9). This might explain the relatively large single channel conductance observed here with 10 mM $Mg^{2+}$ in that these negatively charged glutamates could increase the effective $Mg^{2+}$ concentration close to the pore. Our mutational studies (this work; (14,26)) are consistent with this notion, yet we presently cannot decide whether the charge of residues or their effect on folding structures of the loop is predominant. $Mg^{2+}$ uptake studies with isolated mitochondria indicated that Mrs2p activity may be regulated directly or indirectly by the matrix $Mg^{2+}$ concentration (4,7). Here we provided strong evidence for matrix $Mg^{2+}$ interfering with the Mrs2p channel activity. Physiological concentrations of 1 mM $Mg^{2+}$ have been found to strongly reduce the open probability of Mrs2p channels suggesting an intrinsic negative feedback mechanism. In accordance, binding of $Mg^{2+}$ to the N-terminal part of CorA was proposed to elicit conformational changes transmitted through long helices ($\alpha5$, $\alpha6$, $\alpha7$) to regulate pore opening (4,9).

Insertion (Mrs2-HA(ins207/208)) and deletion (Mrs2-HA(Δ277–282)) studied here affect putative coiled-coil domains of Mrs2p helices equivalent to helices $\alpha5/\alpha6$ and $\alpha7$, respectively, of the CorA crystal structure. These helices have been proposed to undergo conformational changes during transition between open and closed states of the CorA pore (4,8,9). Accordingly, any insertion of seven amino acids (Mrs2-HA(ins207/208) as well as deletion of six amino acids (Mrs2-HA(Δ277–282)) might be expected to significantly change the channel characteristics. In fact, those mutant Mrs2p channels exhibited a range of exceptional open states and current amplitudes consistent with disturbed $Mg^{2+}$ permeation. Mutant Mrs2 insertion and deletion protein oligomers also had reduced stability when assayed in BN electrophoresis. Further studies will be necessary to decide whether the increased open probability of the mutant channels results from lowered stability of the Mrs2 oligomers or from structural changes in the monomers, or from both. Taken together, access of $Mg^{2+}$ to the N-terminal (matrix) side of Mrs2p and changes in helices of this part of the protein can considerably affect the gating as well as the permeation of the channel.

The presence of a high conductance $Mg^{2+}$ channel in mitochondria is surprising given that the steady-state $[Mg^{2+}]$ concentrations in mitochondria and cytoplasm appear to be similar (33). We speculate that physiological conditions exist in these organelles that create a sudden requirement for $Mg^{2+}$, which can only be met by a high conductance channel. The binding constant of $Mg^{2+}$ to ATP is almost an order of magnitude higher than to ADP. Mitochondrial ATP concentrations vary considerably depending on the physiological state of cells and can rise to 0.2 mM (34). Given that $[Mg^{2+}]_m$ is in a range of 0.4–0.8 mM (33), a burst in ATP synthesis would result in binding of considerable part of free ionized $Mg^{2+}$ to ATP, and this event in turn may trigger rapid influx of $Mg^{2+}$. In fact, $[Mg^{2+}]_m$ of isolated mammalian mitochondria has been shown to increase by $>30\%$ upon addition of ADP, which stimulates respiratory activity and ATP synthesis (35).

In conclusion, data presented here for yeast Mrs2p unequivocally revealed that a member of the CorA-related proteins forms a high-conductance $Mg^{2+}$ channel. We thus speculate that the bacterial members of this superfamily of $Mg^{2+}$ transporters act as channels, first because Mrs2 and Alr1 proteins apparently share structural features of their core sequences with CorA proteins (4) and second, because effects of mrs2 mutations on channel activity match very well predictions based on the crystal structure of CorA.

Electrophysiological measurements of ion conductance of CorA proteins will be necessary to finally determine their mode and capacity of ion transport.

## SUPPLEMENTARY MATERIAL

To view all of the supplemental files associated with this article, visit www.biophysj.org.

We thank Dr. Oliviero Carugo for helpful suggestions on structural alignments of Mrs2p and CorA.

This work was supported by the Austrian Science Fund and the Vienna Science and Technology Fund. The authors disclose any financial interest that might be construed to influence the results or interpretation of this manuscript.

## REFERENCES

1. Gardner, R. C. 2003. Genes for magnesium transport. *Curr. Opin. Plant Biol.* 6:263–267.

2. Knoop, V., M. Groth-Malonek, M. Gebert, K. Eifler, and K. Weyand. 2005. Transport of magnesium and other divalent cations: evolution of the 2-TM-GxN proteins in the MIT superfamily. *Mol. Genet. Genomics*. 274:205–216.

3. Maguire, M. E. 2006. The structure of CorA: a $Mg^{2+}$-selective channel. *Curr. Opin. Struct. Biol*. 16:432–438.

4. Lunin, V. V., E. Dobrovetsky, G. Khutoreskaya, R. Zhang, A. Joachimiak, D. A. Doyle, A. Bochkarev, M. E. Maguire, A. M. Edwards, and C. M. Koth. 2006. Crystal structure of the CorA $Mg^{2+}$ transporter. *Nature*. 440:833–837.

5. Smith, R. L., and M. E. Maguire. 1998. Microbial magnesium transport: unusual transporters searching for identity. *Mol. Microbiol.* 28: 217–226.

6. Froschauer, E., K. Nowikovsky, and R. J. Schweyen. 2005. Electroneutral $K^+/H^+$ exchange in mitochondrial membrane vesicles involves Yo1027/Letm1 proteins. *Biochim. Biophys. Acta*. 1711:41–48.

7. Kolisek, M., G. Zsurka, J. Samaj, J. Weghuber, R. J. Schweyen, and M. Schweigel. 2003. Mrs2p is an essential component of the major electrophoretic $Mg^{2+}$ influx system in mitochondria. *EMBO J*. 22:1235–1244.

8. Eshaghi, S., D. Niegowski, A. Kohl, D. Martinez Molina, S. A. Lesley, and P. Nordlund. 2006. Crystal structure of a divalent metal ion transporter CorA at 2.9 angstrom resolution. *Science*. 313:354–357.

9. Payandeh, J., and E. F. Pai. 2006. A structural basis for $Mg^{2+}$ homeostasis and the CorA translocation cycle. *EMBO J*. 25:3762–3773.

10. Nadler, M. J., M. C. Hermosura, K. Inabe, A. L. Perraud, Q. Zhu, A. J. Stokes, T. Kurosaki, J. P. Kinet, R. Penner, A. M. Scharenberg, and A. Fleig. 2001. LTRPC7 is a Mg.ATP-regulated divalent cation channel required for cell viability. *Nature*. 411:590–595.

11. Maguire, M. E. 2006. Magnesium transporters: properties, regulation and structure. *Front. Biosci.* 11:3149–3163.

12. Goytain, A., R. M. Hines, A. El-Husseini, and G. A. Quamme. 2007. NIPA1(SPG6), the basis for autosomal dominant form of hereditary spastic paraplegia, encodes a functional $Mg^{2+}$ transporter. *J. Biol. Chem.* 282:8060–8068.

13. Bui, D. M., J. Gregan, E. Jarosch, A. Ragnini, and R. J. Schweyen. 1999. The bacterial magnesium transporter CorA can functionally substitute for its putative homologue Mrs2p in the yeast inner mitochondrial membrane. *J. Biol. Chem.* 274:20438–20443.

14. Wachek, M., M. C. Aichinger, J. A. Stadler, R. J. Schweyen, and A. Graschopf. 2006. Oligomerization of the $Mg^{2+}$-transport proteins Alr1p and Alr2p in yeast plasma membrane. *FEBS J*. 273:4236–4249.

15. Gregan, J., M. Kolisek, and R. J. Schweyen. 2001. Mitochondrial $Mg^{2+}$ homeostasis is critical for group II intron splicing in vivo. *Genes Dev*. 15:2229–2237.

16. Zsurka, G., J. Gregan, and R. J. Schweyen. 2001. The human mitochondrial Mrs2 protein functionally substitutes for its yeast homologue, a candidate magnesium transporter. *Genomics*. 72:158–168.

17. Wiesenberger, G., M. Waldherr, and R. J. Schweyen. 1992. The nuclear gene MRS2 is essential for the excision of group II introns from yeast mitochondrial transcripts in vivo. *J. Biol. Chem*. 267:6963–6969.

18. Gregan, J., D. M. Bui, R. Pillich, M. Fink, G. Zsurka, and R. J. Schweyen. 2001. The mitochondrial inner membrane protein Lpe10p, a homologue of Mrs2p, is essential for magnesium homeostasis and group II intron splicing in yeast. *Mol. Gen. Genet*. 264:773–781.

19. Pogulis, R. J., A. N. Vallejo, and L. R. Pease. 1996. In vitro recombination and mutagenesis by overlap extension PCR. *Methods Mol. Biol.* 57:167–176.

20. Schagger, H., W. A. Cramer, and G. von Jagow. 1994. Analysis of molecular masses and oligomeric states of protein complexes by blue native electrophoresis and isolation of membrane protein complexes by two-dimensional native electrophoresis. *Anal. Biochem*. 217:220–230.

21. Criado, M., and B. U. Keller. 1987. A membrane-fusion strategy for single-channel recordings of membranes usually non-accessible to patch-clamp pipette electrodes. *FEBS Lett*. 224:172–176.

22. Riquelme, G., E. Lopez, L. M. Garcia-Segura, J. A. Ferragut, and J. M. Gonzalez-Ros. 1990. Giant liposomes: a model system in which to obtain patch-clamp recordings of ionic channels. *Biochemistry*. 29:11215–11222.

23. Hamill, O. P., A. Marty, E. Neher, B. Sakmann, and F. J. Sigworth. 1981. Improved patch-clamp techniques for high-resolution current recording from cells and cell-free membrane patches. *Pflugers Arch*. 391:85–100.

24. Reinsprecht, M., M. H. Rohn, R. J. Spadinger, I. Pecht, H. Schindler, and C. Romanin. 1995. Blockade of capacitive $Ca^{2+}$ influx by $Cl^-$ channel blockers inhibits secretion from rat mucosal-type mast cells. *Mol. Pharmacol*. 47:1014–1020.

25. Kucharski, L. M., W. J. Lubbe, and M. E. Maguire. 2000. Cation hexaammines are selective and potent inhibitors of the CorA magnesium transport system. *J. Biol. Chem.* 275:16767–16773.

26. Weghuber, J., F. Dieterich, E. M. Froschauer, S. Svidova, and R. J. Schweyen. 2006. Mutational analysis of functional domains in Mrs2p, the mitochondrial $Mg^{2+}$ channel protein of *Saccharomyces cerevisiae*. *FEBS J*. 273:1198–1209.

27. Schagger, H., and G. von Jagow. 1991. Blue native electrophoresis for isolation of membrane protein complexes in enzymatically active form. *Anal. Biochem*. 199:223–231.

28. Kirichok, Y., G. Krapivinsky, and D. E. Clapham. 2004. The mitochondrial calcium uniporter is a highly selective ion channel. *Nature*. 427:360–364.

29. Lohret, T. A., and K. W. Kinnally. 1995. Multiple conductance channel activity of wild-type and voltage-dependent anion-selective channel (VDAC)-less yeast mitochondria. *Biophys. J*. 68:2299–2309.

30. Szabo, I., J. Bock, A. Jekle, M. Soddemann, C. Adams, F. Lang, M. Zoratti, and E. Gulbins. 2005. A novel potassium channel in lymphocyte mitochondria. *J. Biol. Chem.* 280:12790–12798.

31. Monteilh-Zoller, M. K., M. C. Hermosura, M. J. Nadler, A. M. Scharenberg, R. Penner, and A. Fleig. 2003. TRPM7 provides an ion channel mechanism for cellular entry of trace metal ions. *J. Gen. Physiol*. 121:49–60.

32. Kozak, J. A., H. H. Kerschbaum, and M. D. Cahalan. 2002. Distinct properties of CRAC and MIC channels in RBL cells. *J. Gen. Physiol*. 120:221–235.

33. Romani, A., C. Marfella, and A. Scarpa. 1993. Cell magnesium transport and homeostasis: role of intracellular compartments. *Miner. Electrolyte Metab*. 19:282–289.

34. Gajewski, C. D., L. Yang, E. A. Schon, and G. Manfredi. 2003. New insights into the bioenergetics of mitochondrial disorders using intracellular ATP reporters. *Mol. Biol. Cell*. 14:3628–3635.

35. Jung, D. W., L. Apel, and G. P. Brierley. 1990. Matrix free $Mg^{2+}$ changes with metabolic state in isolated heart mitochondria. *Biochemistry*. 29:4121–4128.

36. Baumann, F., W. Neupert, and J. M. Herrmann. 2002. Insertion of bitopic membrane proteins into the inner membrane of mitochondria involves an export step from the matrix. *J. Biol. Chem.* 277:21405–21413.